Journal of Materials Chemistry C

ROYAL SOCIETY OF CHEMISTRY

PAPER

View Article Online
View Journal | View Issue

Cite this: J. Mater. Chem. C, 2022, 10, 12436

Using chiral ammonium cations to modulate the structure of 1D hybrid lead bromide perovskites for linearly polarized broadband light emission at room temperature†

Joanna M. Urban, ‡[a] Abdelaziz Jouaiti, *[b] Nathalie Gruber, [b] Géraud Delport, [c] Gaëlle Trippé-Allard,[a] Jean-François Guillemoles, [c] Emmanuelle Deleporte, [a] Sylvie Ferlay *[b] and Damien Garrot *[d]

We report on a series of low dimensional 1D enantiomerically pure and racemic lead bromide perovskite compounds of the formula **BuA**-$PbBr_3$, **MBA**-$PbBr_3$ and **EBA**-$PbBr_3$ (**BuA**, cation derived from 2-Butylamine, **MBA** from Methylbenzylamine and **EBA** from α-Ethylbenzylamine) incorporating monovalent chiral ammonium derivative cations. A series of 6 enantiomerically pure compounds is described. The compounds are fully characterized from a structural point of view using X-Ray diffraction on single crystals and XRPD. Their photoluminescence emission properties have been carefully investigated. The use of cations of different sizes allows tuning the distances between the inorganic one-dimensional (1D) chains. All compounds show broadband below-bandgap emission, attributed to Self-Trapped Exciton (STE) recombination. The photoluminescence is characterized by a significant degree of linear polarization at room temperature, which can be explained by the structural anisotropy of the transition dipole moments and quantum confinement of the excitons in the 1D material. Our results indicate that the described compounds are of high interest for linearly-polarized broadband light-emitting devices and demonstrate the possibility of engineering the crystalline structure by the appropriate choice of the organic cation.

Received 17th May 2022,
Accepted 9th August 2022

DOI: 10.1039/d2tc02040h

rsc.li/materials-c

Introduction

Hybrid organic–inorganic perovskites (HOIPs) are a class of crystalline semiconductor materials displaying tunable structures of varying dimensionality.[1–5] Their remarkable opto-electronic properties, including large absorption coefficients[6] and long carrier diffusion lengths,[7] make HOIPs promising candidates for applications requiring high quantum efficiency, most notably as light-harvesting materials for photovoltaics[1,2,6] as well as active materials in light-emitting devices and photodetectors.[8] The HOIP lattice is built from large organic cations and an inorganic network (large metal cations (Pb^{2+}, Bi^{3+}, ...) and halide anions). The structural features and photophysical properties of the material can be tailored by varying the ionic composition.[9] Generally, introducing large organic cations which violate the Goldschmidt tolerance factor into the lattice[10] disrupts the 3D structure, leading to the formation of lower dimensional 1D or 2D perovskite materials with optoelectronic characteristics different from their 3D analogs.

While the majority of reported lead halide perovskite belongs either to the layered 2D or 3D class,[4] interest in 1D halide perovskites[11,12] has recently been growing due to their inherent one-dimensional character, which can enhance charge carrier transport along a particular direction,[13] as well as their typically high crystallinity and consequently high quantum efficiencies and long carrier diffusion lengths,[11] which are of prime importance for the performance of perovskite-based nanoscale optoelectronic and photonic devices.[14–17] The structural anisotropy of

[a] Université Paris-Saclay, ENS Paris-Saclay, CentraleSupélec, CNRS, UMR 9024, LuMIn, 91190, Gif-sur-Yvette, France
[b] Université de Strasbourg-CNRS, UMR 7140, F-67000, Strasbourg, France. E-mail: ferlay@unistra.fr, jouaiti@unistra.fr
[c] IPVF, CNRS, UMR 9006 IPVF Institut Photovoltaïque d'Ile-de-France 18 Boulevard Thomas Gobert, Palaiseau 91120, France
[d] Université Paris-Saclay, UVSQ, CNRS, GEMaC, 78000, Versailles, France. E-mail: damien.garrot@universite-paris-saclay.fr

† Electronic supplementary information (ESI) available: XRPD diagrams for all the compounds, UV diffuse spectra, CD spectra, integrated intensity of the broad emission peak for all the compound, photoluminescence spectra as a function of excitation power for the (*R*)-**BuA**-$PbBr_3$, Table of X-ray crystallographic data collection, distances and bonds for the studied compounds and structural analysis using shape program. CCDC 2167649–2167656. For ESI and crystallographic data in CIF or other electronic format see DOI: https://doi.org/10.1039/d2tc02040h

‡ Currently at Fritz Haber Institute of the Max Planck Society, 14195 Berlin, Germany.

perovskite structures with lowered dimensionality manifests in their electronic and optical properties and makes them highly attractive for polarization-sensitive optoelectronic devices.[18] In addition, broadband emission in the visible range with high potential for white light emission applications has been recently observed for low-dimensional perovskite materials.[3,19–21,28] It is generally believed that exciton self-trapping (Self-Trapped Excitons, STE) in the strongly distorted lattice lies at the origin of such broadband photoluminescence.[3,19,22,23] The chromaticity of the emission can be tuned, for example, by varying the nature of the halogen,[24] making low-dimensional HOIPs promising white light emitters.

In lower-dimensional perovskite structures, optoelectronic properties can be controlled by the choice of cations with specific functionality. For example, chiroptical properties can be transferred to the perovskite structure by the intercalation of chiral cationic organic compounds.[18,25–29] In the last five years, the interest in **c**hiral Hybrid Organic–Inorganic Perovskites (*c*-HOIP) has grown, mainly due to their intriguing physical properties including nonlinear optical responses, circular dichroism, ferroelectricity, circularly polarized light absorption and emission and spin dependent transport.[30–32]

1D *c*-HOIPs perovskites combine the advantages of chiral materials and low-dimensional lead halide perovskite structures and hold promise for a wide range of applications in life science, material science and in next-generation optical and spintronic devices.[26,30]

In this work, we report the synthesis of one-dimensional compounds incorporating chiral (and for some of them racemic) cations derived from 2-butylamine, **BuA** (cation **BuA**H^+, in the following called **BuA**), Methylbenzylamine, **MBA** and α-Ethylbenzylamine, **EBA**, represented in Fig. 1. The choice of these cations is guided by their availability and ability to form 1D structures with lead perovskites. After a careful structural study series of 6 enantiomerically pure compounds and for two of them the racemic compounds, we characterize their photoluminescence properties and observe a broadband yellow to orange emission with a significant degree of linear polarization.

Results and discussion

Structural characterization

Three pairs of enantiomeric cations have been used in the following study. **BuA**, **MBA** and **EBA** are monovalent cationic species (see Fig. 1). To the best of our knowledge, lead-halide structures with **BuA** or **EBA** cations have not been reported previously. Concerning the **MBA** amine, several 1D structures have been already reported, among them the structure consisting of *R*-MBA combined with a $PbCl_3$, $PbBr_3$[33] or PbI_3 inorganic sublattice and *R*-**MBA** and *S*-**MBA**[25,34] as well as the racemic mixture of the cations combined with the PbI_3 sublattice.[14] Other related 2D structures involving mixtures of PbI_4 and $PbBr_4$ have also been reported.[28]

The enantiomeric compounds (*S*) and (*R*)-of **BuA**-$PbBr_3$, **MBA**-$PbBr_3$ and **EBA**-$PbBr_3$ are all isomorphous, crystallizing in the $P2_12_12_1$ space group (see crystallographic Table S1, ESI†), belonging to non-centrosymmetric Sohncke space groups.

The crystal structure is based on cationic protonated monovalent cations and the anionic inorganic $PbBr_3^-$ chains formed by face-sharing metal-halide octahedral. The compounds have one-dimensional character on the molecular level, in contrast to materials with 3D stoichiometry where the low-dimensional character is due to purely morphological confinement.[35] For the six reported compounds, the inorganic chains are distorted (see Fig. 2) and the metal cations are in a distorted octahedral environment as shown by angles and distances reported in Table S2, ESI,† and as demonstrated by the Shape analysis detailed below. The inorganic units are not helicoidal and thus not intrinsically chiral.

In the unit cell, the 1D bromoplumbate arrays are separated by the chiral amines, as shown in Fig. 3, with an alternate disposition of the protonated amino groups. Within the unit cells, there are some hydrogen bonds formed between the amino groups and the Br atoms, with the N···Br distances in the 3.3940(13)–3.6653(13) Å range, as shown in Table S2, ESI.†

1D compounds including cyclohexane (rather than phenyl) derivative amines have been reported not only for the *R* and *S* enantiomers but also for their racemic mixtures.[36] For this reason, the synthesis and characterization of the racemic analogs of the three enantiomeric compounds have been undertaken. The structures of the racemic (*rac*)-**BuA**-$PbBr_3$ and (*rac*)-**EBA**-$PbBr_3$ compounds are analogous to the ones reported for the corresponding enantiomers. (*rac*)-**MBA**-$PbBr_3$ reproducibly crystallizes into another phase, including solvent molecules. Despite many attempts, we were not able to obtain an achiral phase structurally analogous to the ones observed for (*S*)-**MBA**-$PbBr_3$ or (*R*)-**MBA**-$PbBr_3$. The formation of a different phase for a racemic mix of the organic large cation molecules was previously reported for other lead halogen perovskites with chiral amino based cations and explained by a different packing of the molecules within the structure.[3,37]

For the **BuA** and **EBA** cations, the corresponding racemic compounds crystallize in centrosymmetric space groups (*monoclinic* $P2_1/n$ for (*rac*)-**BuA**-$PbBr_3$, and *orthorhombic Pnma* for

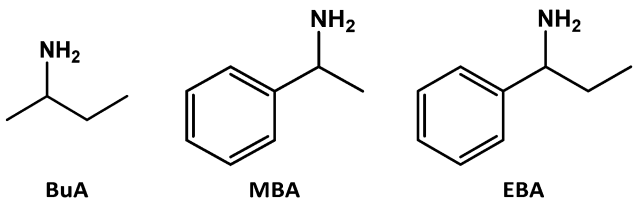

Fig. 1 The amines used for the formation of lead-bromide species **BuA**-$PbBr_3$, **MBA**-$PbBr_3$ and **EBA**-$PbBr_3$.

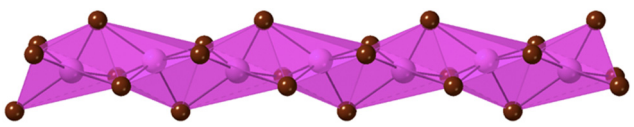

Fig. 2 Schematical polyhedral representation of one $PbBr_3^-$ anionic inorganic chain in the **BuA**-$PbBr_3$, **MBA**-$PbBr_3$ and **EBA**-$PbBr_3$ compounds.

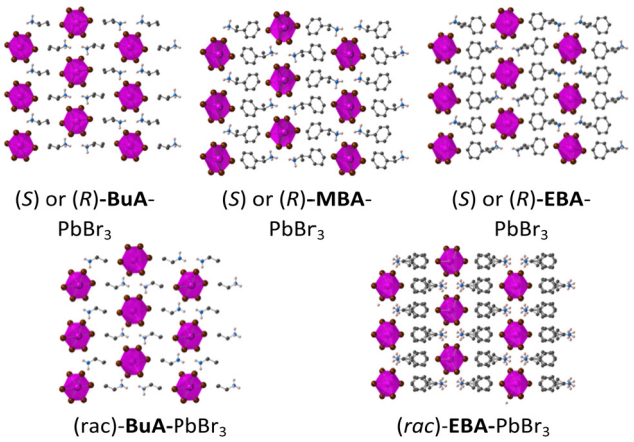

Fig. 3 Representation of the structures of either (*S*)- or (*R*)-**BuA**-$PbBr_3$, **MBA**-$PbBr_3$, **EBA**-$PbBr_3$, (*rac*)-**BuA**-$PbBr_3$ and (*rac*)-**EBA**-$PbBr_3$, projection in the xOz planes. Only H atoms located on N are presented. For bond and distances see text.

(*rac*)-**EBA**-$PbBr_3$). For both compounds, the $PbBr_3^-$ anionic chains (analog to the ones of the enantiomerically pure compounds, represented in Fig. 2) and the ammonium cations are present in the unit cell, without solvent molecules (see Fig. 3). For (*rac*)-**EBA**-$PbBr_3$, the organic cations appear to be disordered. Bonds and distances are reported in Table S2 (ESI†). As in the case of enantiomeric compounds, there are weak specific interactions between Br and N protonated atoms, with N-Br distance shown in Table S2, ESI.†

The spacing between the inorganic $PbBr_3^-$ arrays in the unit cell has been measured for all the compounds and the distances are reported in Table 1. They are increasing in accordance with the size of the used cation when going from **BuA** to **MBA** then to **EBA**.

The analysis of the distortions around the Pb^{2+} cations in the 1D compounds has been performed using the Shape program.[38,39]

The octahedral distortion determined using a $PbBr_6$ O_h model is high (with CShM (Continuous Shape Measures) values varying between 14.013 and 19.070 (see ESI†)). These values are high when compared to other values provided for 2D lead halides perovskites,[40] but we can assume a more distorted environment for 1D inorganic compounds. A careful analysis of the Pb–Br distances (see Table S2, ESI†) shows that a shorter Pb–Br distance (varying between 3.2382(10) and 3.4549(13) Å, for the 8 considered compounds) is observed for the Pb^{2+} cations in compounds presenting the highest CShM values towards octahedral $PbBr_6$ environment ((*S*)-**BuA**-$PbBr_3$, (*R*)-**BuA**-$PbBr_3$, *rac*-**BuA**-$PbBr_3$). The series of compounds with the **BuA** cation present the smaller deviation and the series with **EBA** and **MBA** cations present higher deviations. Interestingly, considering a $PbBr_5$ environment around the metal cations, (C_{4v} point group) as the undistorted structure (square pyramidal or truncated octahedral geometry), the calculations indicate that the series associated with the cations **EBA** and **MBA** present the smallest deviations. We can conclude that (*S*)-**BuA**-$PbBr_3$, (*R*)-**BuA**-$PbBr_3$ and *rac*-**BuA**-$PbBr_3$ present a strongly distorted octahedral geometry whereas (*S*)-**MBA**-$PbBr_3$, (*R*)-**MBA**-$PbBr_3$, (*S*)-**EBA**-$PbBr_3$, (*R*)-**EBA**-$PbBr_3$ and *rac*-**EBA**-$PbBr_3$ present a geometry closer to square pyramidal.

Table 1 Distances between the 1D lead bromide units for (*S*)- or (*R*)-**BuA**-$PbBr_3$, **MBA**-$PbBr_3$, **EBA**-$PbBr_3$, (*rac*)-**BuA**-$PbBr_3$ and (*rac*)-**EBA**-$PbBr_3$

	Distance between two arrays (Å) $c/2$ and b (or a)
(*R*)-**BuA**-$PbBr_3$	8.905 and 7.954
(*S*)-**BuA**-$PbBr_3$	8.921 and 7.968
rac-**BuA**-$PbBr_3$	8.812 and 7.971
(*R*)-**MBA**-$PbBr_3$	10.131 and 7.886
(*S*)-**MBA**-$PbBr_3$	10.148 and 7.902
(*R*)-**EBA**-$PbBr_3$	10.250 and 8.174
(*S*)-**EBA**-$PbBr_3$	10.2620 and 8.177
rac-**EBA**-$PbBr_3$	10.651 and 8.019

The resulting polycrystalline powders were analyzed using PXRD for all the compounds. The PXRD diagrams of all the polycrystalline samples evidence a good match between the simulated and experimental patterns, as shown in Fig. S1 (ESI†), confirming that the microcrystalline powders do not exhibit traces of impurities or other crystalline phases.

Optical characterization

The reflectance-UV spectra for the pairs of (*S*) and (*R*) **BuA**-$PbBr_3$, **MBA**-$PbBr_3$ and **EBA**-$PbBr_3$ enantiomers (Fig. S2, ESI†) display an optical band gap lying between 2.8 and 3.4 eV.

The photoluminescence (PL) spectra measured under 325 nm (3.815 eV) continuous-wave excitation on large (mm-sized) crystals of the *R*- and *S*-enantiomer based compounds are shown in Fig. 4a. All samples show a very broad emission spectrum with a maximum at around 1.9–2.0 eV, corresponding to a significant Stokes shift of above 1 eV, consistent with previous reports for STE emission[19,23] and earlier observations for the **MBA**-$PbBr_3$ compound.[34] The excitonic character of the broad emission band is confirmed by the linear dependence of the integrated intensity on the excitation power for all of the investigated compounds, in agreement with what has previously been reported for STE emission.[19,23] In contrast, a saturation at high excitation intensity would be expected for defect-related PL features. Fig. 4b shows the excitation power dependence of the integrated emission intensity for the (*R*) enantiomers of the different compounds. The full set of data is presented in Fig. S3, ESI.† This allows to rule out defect-related character of the broad PL band,[41] for which a sub-linear dependence should be observed. It should be noticed that no changes of spectral shape can be observed when increasing the excitation power (see Fig. S4, ESI†), ruling out donor-acceptor pair emission or defect saturation effects.

The maximum of the emission is slightly spectrally shifted for the different compounds and a shoulder at around 2.5 eV is observed only for the **EBA**-$PbBr_3$ crystal. It is possibly related to a local impurity although we cannot exclude the presence of a different emissive self-localized state at higher energy.[42] The Stokes-shifted emission was dominant and no significant signal related to the recombination of FE (Free Excitons) could be well resolved. The presence of an energy barrier separating the FE and STE states can explain the quenching of the FE emission

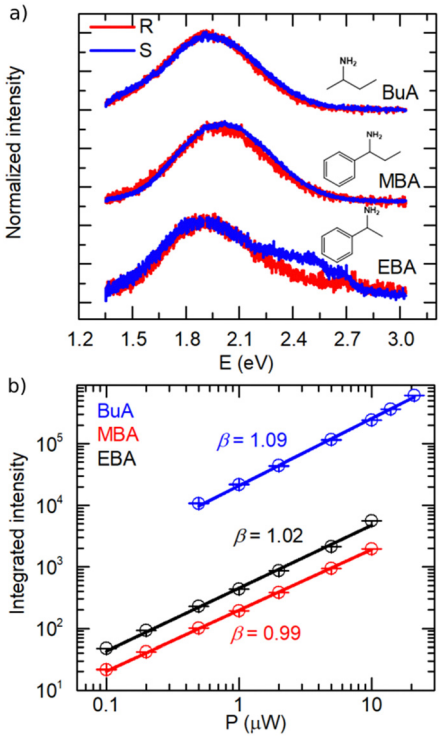

Fig. 4 (a) PL emission spectra of (*S*)- or (*R*)-**BuA**-$PbBr_3$, **MBA**-$PbBr_3$ and **EBA**-$PbBr_3$ compounds measured using 325 nm (3.815 eV) excitation. (b) Integrated intensity of the broad emission peak as a function of the 3.06 eV excitation power for the (*R*) enantiomers of the three compounds. The experimental data is marked in blue (**BuA**-$PbBr_3$), red (**MBA**-$PbBr_3$) and black (**EBA**-$PbBr_3$) symbols. The lines show the fit of the power law $I = aP^{\beta}$.

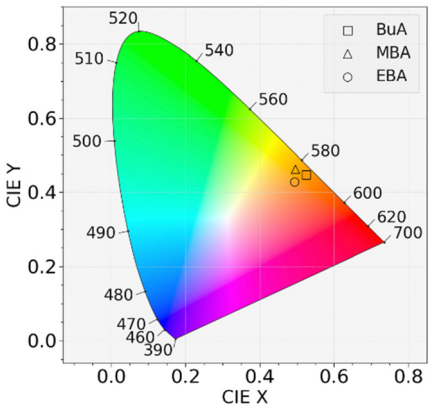

Fig. 5 The CIE coordinates for (*S*)- or (*R*)-**BuA**-$PbBr_3$, **MBA**-$PbBr_3$ and **EBA**-$PbBr_3$ compounds. Because of the spectral similarity of the emission for the (*R*) and (*S*) enantiomers, only the coordinates calculated for the (*R*)-enantiomer compounds are shown for better clarity.

and the presence of only STE emission at elevated temperatures.[21,23] The observation of a broadband STE emission at room temperature could be correlated with the observed octahedral distortion. In 2D hybrid perovskite, the intensity of the STE emission relative to the FE emission is found to increase linearly with the out of plane distortion of the Pb-(μ-X)-Pb (X = Cl^-/Br^-) angle in the inorganic sheet.[43] It has been established that the broadening and the intensity of the photoluminescence emission spectrum of low dimensional HOIPs (mainly 2D) are strongly related with the distortion around the metal cations[40] and also in the inorganic lattice.[43]

To further characterize the broadband emission, the Commission Internationale de l'Eclairage (CIE) chromaticity coordinates of enantiomerically pure compounds were determined. The CIE chromaticity coordinates (Fig. 5) were determined as (0.53, 0.45) for **BuA**-$PbBr_3$, (0.50, 0.46) for **MBA**-$PbBr_3$ and (0.49, 0.43) for **EBA**-$PbBr_3$, corresponding to a larger contribution in the orange-red region of the spectrum. The Correlated Color Temperatures (CCT) were determined as 2238 K, 2620 K and 2404 K for the **BuA**-, **MBA**- and **EBA** compounds, respectively. Broadband emission at such low energy spectral range has recently been reported for other 1D perovskite compounds[44,45] as well as for 0D metal halides[46] and 0D mixed halide perovskites[47] and is considered highly interesting for applications in light-emitting devices.[44,47]

Comparing the PL emission spectra obtained using 3.18 eV and 3.06 eV excitation (Fig. S4, ESI†), we observed a blueshift of the broadband emission for lower excitation energy, which is consistent with previous observations for STE emission in low-dimensional perovskites and could indicate the existence of multiple STE states with different energies.[23]

We have also investigated the polarization properties of the diffuse reflectance and PL emission. The diffuse reflectance circular dichroism (DRCD) spectra for the pairs of (*S*) and (*R*)-**BuA**-$PbBr_3$, **MBA**-$PbBr_3$ and **EBA**-$PbBr_3$ enantiomers are presented in Fig. S5 (ESI†). They attest the presence of enantiomers in the crystalline phase of each compound.

We then analyzed the degree of linear polarization of the broadband emission for the (*R*)-**BuA**-$PbBr_3$, (*S*)-**BuA**-$PbBr_3$ and (*rac*)-**BuA**-$PbBr_3$ compounds. Due to the 1D structure of the compounds, comparable to the structure of quantum wires, a significant anisotropy of the PL emission can be expected.

Fig. 6 shows the normalized integrated emission intensity as a function of the orientation of the linear polarization analyzer. The data can be fitted by the Malus' law: $I(\theta) = I_0 + A\cos^2(\theta - \theta_0)$ and the DLP (Degree of Linear Polarization) is defined as $(A)/(A + 2I_0)$. The DLP is 24% for (*R*)-**BuA**-$PbBr_3$, 45% for the (*S*)-**BuA**-$PbBr_3$ and 15% for (*rac*)-**BuA**-$PbBr_3$, which is significant for a bulk crystal at room temperature.[18]

No detectable circular polarization of the PL could be measured, once we exclude any artifacts that could arise due to the presence of linear polarization.[48] Enhanced carrier-phonon interaction and thermal lattice expansion at elevated temperatures, as well as increased probability of a spin-flip may explain the absence of circular polarization at room temperature.[49]

High degrees of linear polarization can be achieved for PL emission from individual nanowires and nanocrystals.[50–53] However, to achieve polarized emission at the macroscopic scale, the synthesis of composite structures is generally required, such as nanocrystals embedded in stretched polymer films (polarization ratio of around 30%)[54] or dispersed in nematic liquid crystals (PL anisotropies up to 30%).[55] Here,

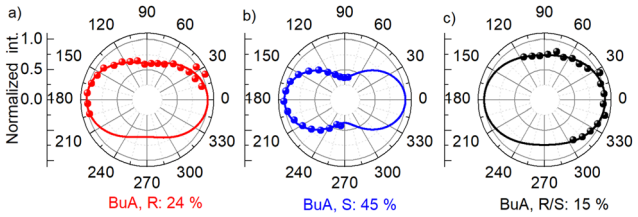

Fig. 6 Polar plots of the normalized intensity of the photoluminescence emission as a function of detection angle measured for 3.815 eV excitation for (a) (*R*)-**BuA**-$PbBr_3$, (b) (*S*)-**BuA**-$PbBr_3$ and (c) (*rac*)-**BuA**-$PbBr_3$.

we observe a significant linear polarization from macroscopic crystals which can be explained by the intrinsic anisotropy of the transition dipole moments and quantum confinement effects as well as additional anisotropic distortions of the octahedral of the inorganic lattice responsible for the self-trapping in the 1D structure.[43] The presence of significant DLP in macroscopic single crystals proves good crystalline quality since the presence of differently oriented crystalline domains would lead to the loss of correlation between the macroscopic long axis of a crystal and the linear polarization direction.[18] In this context, our observation of strong linear polarization in macroscopic crystals is interesting from the point of view of potential applications in polarized light emission[56,57] and detection.[58]

Conclusions

In this work, we investigated the formation of a series of chiral 1D perovskites built from $PbBr_3$ and ammonium based enantiomerically pure cations (**BuA**, **MBA** and **EBA**) inserted between the 1D inorganic arrays. For **BuA** and **EBA**, the analogous racemic compounds were obtained, and they present the same structural arrangement as for the pure enantiomers. Broadband below-gap photoluminescence was observed for all of the synthesized perovskite compounds and attributed to the recombination of self-trapped excitons. The yellow to orange spectral range of the STE emission makes the investigated compounds highly interesting for light-emitting devices such as optically pumped LEDs, where they could be used in combination with blue-emitting phosphors to obtain a high color rendering index and overcome the issue of deficiency in red emission encountered for many yellow phosphors.[47]

For all enantiomers of the **BuA**-based compound, polarization-resolved PL emission measurements evidence a significant linear polarization at RT as the consequence of the structural anisotropy of the 1D crystal structure. Broadband polarized light sources are highly in demand for applications for display, imaging and optical communications devices[59] and the compounds described in this work expand the new family of polarized broadband light-emitting perovskite materials. Our results provide an example of how the structural distortions and the resulting photophysical properties can be driven by a targeted choice of the organic cations in low-dimensional HOIPs.

Experimental

Synthesis

All chemicals and reagents (starting amine) were of analytical grade and used as received from commercial sources (Sigma-Aldrich). The solvent used in these syntheses was distilled water.

Crystals of (*S*)-BuA-PbBr3, (*R*)-BuA-PbBr3 and (*rac*)-BuA-PbBr3

To a solution of 0.752g (2.05 mmol) of $PbBr_2$ in 4 ml of a 48% HBr solution, 0.3g (4.1 mmol) of (*R*)-, (*S*)- or (*rac*)-BuA were added. The mixture was stirred at room temperature for 1 h. Ethanol solution was diffused by evaporation into the mixture. Many colorless crystals produced after 24 h were collected and washed by Ethanol and diethyl ether.

Crystals of (*S*)-MBA-PbBr and (*R*)-MBA-PbBr3

To a solution of 0.757g (2.06 mmol) of $PbBr_2$ in 6 mL of a 48% HBr solution, 0.5g (2.35 mmol) of (*R*)-or (*S*)-MBA were added. Then the mixture was heated at 80 °C for 1 h. The clear solution was slowly cooled to room temperature which leads to colorless needles. The crystals were collected and washed by ethanol and diethyl ether.

Crystals of (*S*)-EBA-PbBr3, (*R*)-EBA-PbBr3 and (*rac*)-EBA-PbBr3.

Colorless single crystals were all grown following the procedure described above using the same molar ratios, starting from (*R*)-, (*S*)- or (*rac*)-EBA.

X-Ray data collection

Data were collected at 173(2) K on a Bruker APEX8 CCD Diffractometer equipped with an Oxford Cryosystem liquid N_2 device, using graphite-monochromated Mo-K_α (λ = 0.71073 Å) radiation. For both structures, diffraction data were corrected for absorption. Structures were solved using SHELXS-97 and refined by full matrix least-squares on F^2 using SHELXL-97. The hydrogen atoms were introduced at calculated positions and not refined (riding model). They can be obtained free of charge from the Cambridge Crystallographic Data Centre via https://www.ccdc.cam.ac.uk/datarequest/cif. CCDC (*S*)-**BuA**-$PbBr_3$ (2167654), (*R*)-**BuA**-$PbBr_3$ (2167649), *rac*-**BuA**-$PbBr_3$ (2167653), (*S*)-**MBA**-$PbBr_3$ (2167650), (*R*)-**MBA**-$PbBr_3$ (2167652), (*S*)-**EBA**-$PbBr_3$ (2167655), (*R*)-**EBA**-$PbBr_3$ (2167656), *rac*-**EBA**-$PbBr_3$ (2167651).†

Structural deviations calculations

The structural deviations calculations leading to the obtention of the CShM (Continuous Shape Measures) values have been obtained using the Shape program.[38] Based on a general polyhedral approach, computational details are provided in the literature.[39]

Powder diffraction studies (PXRD)

Diagrams were collected on a Bruker D8 diffractometer using monochromatic Cu-K_α radiation with a scanning range between 4 and 40° using a scan step size of 8° mn^{-1}.

Absorbance

The absorption spectra were measured in the solid-state using a PE Lambda 650 S spectrophotometer at room temperature.

Circular dichroism

Diffused reflectance circular dichroism (DRCD) spectra of crystalline samples were performed on a JASCO J-1500 spectrophotometer equipped with an integrating sphere attachment (DRCD-575 accessory) in the 200–400 nm domain at a scan rate of 100 nm min^{-1} and accumulated twelve times.

The solid samples were diluted with KBr to a concentration of 25% (w/w).

Photoluminescent measurements

All the presented optical measurements were performed under ambient conditions. The photoluminescence spectra measured using 3.815 eV excitation, including the polarization-resolved data, were recorded in a macro-PL setup at 45-degree incidence angle using the a HeCd continuous wave laser for excitation. The signal was collected, dispersed by a spectrometer and detected using a CCD camera. For polarization-resolved measurements, an analyser composed of a waveplate and a linear polarizer was placed in front of the spectrometer in the detection path and the waveplate was rotated to detect different polarization states of the emitted light. We used a half-waveplate for the linear polarization measurements and a quarter waveplate for the circular polarization detection. Based on the analysis of the emission of an unpolarized light source, we determined the precision of our polarization detection to be around 3% accounting for instrumental error and the excitation beam intensity fluctuations.

Measurements using 3.06 eV (405 nm) pulsed picosecond excitation, including power-dependent series, were performed in a micro-PL setup in backscattering configuration. The measurements were performed at 5 MHz excitation repetition rate and the size of the spot in the micro-PL configuration is on the order of 1 μm^2.

Since we do not perfectly control the in-plane orientation of the crystalline axis with respect to the detection plane it is possible that the measured DLP is only a lower bound.[20]

Conflicts of interest

There are no conflicts to declare.

Acknowledgements

Financial support from the University of Strasbourg and the CNRS is acknowledged. Dr Catalin Maxim (University of Bucharest, Romania) is acknowledged for recording reflectance-CD spectra. The work of J. M. Urban, D. Garrot, G. Trippé-Allard and E. Deleporte is financially supported by Agence Nationale de la Recherche: EMIPERO Project ANR-18-CE24-0016.

Notes and references

1 D. A. Egger, A. M. Rappe and L. Kronik, Hybrid Organic–Inorganic Perovskites on the Move, *Acc. Chem. Res.*, 2016, **49**, 573–581.
2 W. Li, Z. Wang, F. Deschler, S. Gao, R. H. Friend and A. K. Cheetham, Chemically diverse and multifunctional hybrid organic–inorganic perovskites, *Nat. Rev. Mater.*, 2017, **2**, 16099.
3 L. Mao, P. Guo, M. Kepenekian, I. Hadar, C. Katan, J. Even, R. D. Schaller, C. C. Stoumpos and M. G. Kanatzidis, Structural Diversity in White-Light-Emitting Hybrid Lead Bromide Perovskites, *J. Am. Chem. Soc.*, 2018, **140**, 13078–13088.
4 P. Gao, A. R. Bin Mohd Yusoff and M. K. Nazeeruddin, Dimensionality engineering of hybrid halide perovskite light absorbers, *Nat. Commun.*, 2018, **9**, 5028.
5 J.-C. Blancon, J. Even, C. C. Stoumpos, M. G. Kanatzidis and A. D. Mohite, Semiconductor physics of organic–inorganic 2D halide perovskites, *Nat. Nanotechnol.*, 2020, **15**, 969–985.
6 J.-P. Correa-Baena, M. Saliba, T. Buonassisi, M. Grätzel, A. Abate, W. Tress and A. Hagfeldt, Promises and challenges of perovskite solar cells, *Science*, 2017, **358**(6364), 739–744.
7 S. D. Stranks, G. E. Eperon, G. Grancini, C. Menelaou, M. J. P. Alcocer, T. Leijtens, L. M. Hertz, A. Petrozza and H. Snaith, Electron-Hole Diffusion Lengths Exceeding 1 Micrometer in an Organometal Trihalide Perovskite Absorber, *Science*, 2013, **342**, 341–344.
8 Y. Fu, H. Zhu, J. Chen, M. P. Hautzinger, X.-Y. Zhu and S. Jin, Metal halide perovskite nanostructures for optoelectronic applications and the study of physical properties, *Nat. Rev. Mater.*, 2019, **4**, 169–188.
9 J. Gebhardt and A. M. Rappe, Mix and Match: Organic and Inorganic Ions in the Perovskite Lattice, *Adv. Mater.*, 2019, **31**, 1802697.
10 G. Kieslich, S. Sun and A. K. Cheetham, Solid-state principles applied to organic–inorganic perovskites: new tricks for an old dog, *Chem. Sci.*, 2014, **5**, 4712–4715.
11 T. Qiu, Y. Hu, F. Xu, Z. Yan, F. Bai, G. Jia and S. Zhang, Recent advances in one-dimensional halide perovskites for optoelectronic applications, *Nanoscale*, 2018, **10**, 20963–20989.
12 K. Hong, Q. Van Le, S. Y. Kim and H. W. Jang, Low-dimensional halide perovskites: review and issues, *J. Mater. Chem. C*, 2018, **6**, 2189–2209.
13 H.-C. Kwon, W. Yang, D. Lee, J. Ahn, E. Lee, S. Ma, K. Kim, S.-C. Yun and J. Moon, Investigating Recombination and Charge Carrier Dynamics in a One-Dimensional Nanopillared Perovskite Absorber, *ACS Nano*, 2018, **12**, 4233–4245.
14 C. Chen, L. Gao, W. Gao, C. Ge, X. Du, Z. Li, Y. Yang, G. Niu and J. Tang, Circularly polarized light detection using chiral hybrid perovskite, *Nat. Commun.*, 2019, **10**, 1927.
15 Y. Zheng, J. Xu and X.-H. Bu, 1D Chiral Lead Halide Perovskites with Superior Second-Order Optical Nonlinearity, *Adv. Opt. Mater.*, 2021, **10**, 2101545.
16 D. Fu, J. Xin, Y. He, S. Wu, X. Zhang, X.-M. Zhang and J. Luo, Chirality-Dependent Second-Order Nonlinear Optical Effect in 1D Organic–Inorganic Hybrid Perovskite Bulk Single Crystal, *Angew. Chem. Int. Ed.*, 2021, **60**, 20021–20026.

17 T. Sheikh, S. Maqbool, P. Mandal and A. Nag, Introducing Intermolecular Cation-π Interactions for Water-Stable Low Dimensional Hybrid Lead Halide Perovskites, *Angew. Chem. Int. Ed.*, 2021, **60**, 18265–18271.
18 X. Wang, Y. Wang, W. Gao, L. Song, C. Ran, Y. Chen and W. Huang, Polarization-Sensitive Halide Perovskites for Polarized Luminescence and Detection: Recent Advances and Perspectives, *Adv. Mater.*, 2021, **33**, 2003615.
19 M. D. Smith and H. I. Karunadasa, White-Light Emission from Layered Halide Perovskites, *Acc. Chem. Res.*, 2018, **51**, 619–627.
20 J. Wang, C. Fang, J. Ma, S. Wang, L. Jin, W. Li and D. Li, Aqueous Synthesis of Low-Dimensional Lead Halide Perovskites for Room-Temperature Circularly Polarized Light Emission and Detection, *ACS Nano*, 2019, **13**, 9473–9481.
21 Y. Liu, C. Wang, Y. Guo, L. Ma, C. Zhou, Y. Liu, L. Zhu, X. Li, M. Zhang and G. Zhao, New lead bromide chiral perovskites with ultra-broadband white-light emission, *J. Mater. Chem. C*, 2020, **8**, 5673–5680.
22 Y. Zhang, Y. Fu, F. Tang and X. Zhang, Exciton Self-Trapping Dynamics in 1D Perovskite Single Crystals: Effect of Quantum Tunnelling, *J. Phys. Chem. Lett.*, 2021, **12**, 4509–4516.
23 A. Yangui, D. Garrot, J. S. Lauret, A. Lusson, G. Bouchez, E. Deleporte, S. Pillet, E. E. Bendeif, M. Castro, S. Triki, Y. Abid and K. Boukheddaden, Optical Investigation of Broadband White-Light Emission in Self-Assembled Organic–Inorganic Perovskite $(C_6H_{11}NH_3)_2PbBr_4$, *J. Phys. Chem. C*, 2015, **119**, 23638–23647.
24 E. R. Dohner, A. Jaffe, L. R. Bradshaw and H. I. Karunadasa, Intrinsic White-Light Emission from Layered Hybrid Perovskites, *J. Am. Chem. Soc.*, 2014, **136**, 13154–13157.
25 D. G. Billing and A. Lemmerer, Synthesis and crystal structures of inorganic-organic hybrids incorporating an aromatic amine with a chiral functional group, *CrystEngComm*, 2006, **8**, 686–695.
26 J. Ahn, E. Lee, J. Tan, W. Yang, B. Kim and J. Moon, A new class of chiral semiconductors: chiral-organic-molecule-incorporating organic–inorganic hybrid perovskites, *Mater. Horiz.*, 2017, **4**, 851–856.
27 Y. Dong, Y. Zhang, X. Li, Y. Feng, H. Zhang and J. Xu, Chiral Perovskites: Promising Materials toward Next-Generation Optoelectronics, *Small*, 2019, **15**, 1902237.
28 J. Ahn, S. Ma, J.-Y. Kim, J. Kyhm, W. Yang, J. A. Lim, N. A. Kotov and J. Moon, Chiral 2D Organic Inorganic Hybrid Perovskite with Circular Dichroism Tunable Over Wide Wavelength Range, *J. Am. Chem. Soc.*, 2020, **142**, 4206–4212.
29 A. Pietropaolo, A. Mattoni, G. Pica, M. Fortino, G. Schifino and G. Grancini, Rationalizing the design and implementation of chiral hybrid perovskites, *Chem*, 2022, **8**, 1231–1253.
30 G. Long, R. Sabatini, M. I. Saidaminov, G. Lakhwani, A. Rasmita, X. Liu, E. H. Sargent and W. Gao, Chiral-perovskite optoelectronics, *Nat. Rev. Mater.*, 2020, **5**, 423–439.
31 J. Ma, H. Wang and D. Li, Recent Progress of Chiral Perovskites: Materials, Synthesis, and Properties, *Adv. Mater.*, 2021, **33**, 2008785.
32 Y. Lu, Q. Wang, R. Chen, L. Qiao, F. Zhou, X. Yang, D. Wang, H. Cao, W. He, F. Pan, Z. Yang and C. Song, Spin-Dependent Charge Transport in 1D Chiral Hybrid Lead-Bromide Perovskite with High Stability, *Adv. Funct. Mater.*, 2021, **31**, 2104605.
33 D. G. Billing and A. Lemmerer, Bis[(*S*)-β-phenethylammonium] tribromoplumbate(II), *Acta Cryst.*, 2003, **E59**, m381–m383.
34 Y. Dang, X. Liu, Y. Sun, J. Song, W. Hu and X. Tao, Bulk Chiral Halide Perovskite Single Crystals for Active Circular Dichroism and Circularly Polarized Luminescence, *J. Phys. Chem. Lett.*, 2020, **11**, 1689–1696.
35 M. Z. Rahaman, S. Ge, C.-H. Lin, Y. Cui and T. Wu, *Small Struct.*, 2021, **2**, 2000062.
36 A. Lemmerer and D. G. Billing, Inorganic–Organic Hybrids Incorporating a Chiral Cyclic Ammonium Cation, *S. Afr. J. Chem.*, 2013, **66**, 262–272.
37 M. Li, F. Fang, X. Huang, G. Liu, Z. Lai, Z. Chen, J. Hong, Y. Chen, R.-J. Wei, G.-H. Ning, K. Leng, Y. Shi and B. Tian, Chiral Ligand-Induced Structural Transformation of Low-Dimensional Hybrid Perovskite for Circularly Polarized Photodetection, *Chem. Mater.*, 2022, **34**, 2955–2962.
38 M. Llunell, D. Casanova, J. Girera, P. Alemany and S. Alvarez, *SHAPE, version 2.1*, Universitat de Barcelona, Barcelona, Spain.
39 S. Alvarez, P. Alemany, D. Casanova, J. Cirera, M. Llunell and D. Avnir, Shape maps and polyhedral interconversion paths in transition metal chemistry, *Coord. Chem. Rev.*, 2005, **249**, 1693–1708.
40 L. Mao, Y. Wu, C. C. Stoumpos, M. R. Wasielewski and M. G. Kanatzidis, White-Light Emission and Structural Distortion in New Corrugated Two-Dimensional Lead Bromide Perovskites, *J. Am. Chem. Soc.*, 2017, **139**, 5210–5215.
41 S. Kahmann, E. K. Tekelenburg, H. Duim, M. E. Kamminga and M. A. Loi, Extrinsic nature of the broad photoluminescence in lead iodide-based Ruddlesden-Popper perovskites, *Nat. Commun.*, 2020, **11**, 2344.
42 J.-Q. Zhao, C.-Q. Jing, J.-H. Wu, W.-F. Zhang, L.-J. Feng, C.-Y. Yue and X.-W. Lei, *J. Phys. Chem. C*, 2021, **125**, 10850–10859.
43 M. D. Smith, A. Jaffe, E. R. Dohner, A. M. Lindenberg and H. I. Karunadasa, Structural origins of broadband emission from layered Pb–Br hybrid perovskites, *Chem. Sci.*, 2017, **8**, 4497–4504.
44 L.-J. Feng, Y.-Y. Zhao, R.-Y. Song and C.-Y. Yue, *Z. Anorg. Allg. Chem.*, 2022, **648**, e202100284.
45 H. Lin, C. Zhou, J. Neu, Y. Zhou, D. Han, S. Chen, M. Worku, M. Chaaban, S. Lee, E. Berkwits, T. Siegrist, M.-H. Du and B. Ma, *Adv. Opt. Mater.*, 2019, **7**, 1801474.
46 Q. Mo, J. Yu, C. Chen, W. Cai, S. Zhao, H. Y. Li and Z. Zang, *Laser Photonics Rev.*, 2022, 2100600.
47 C. Zhou, Y. Tian, Z. Yuan, H. Lin, B. Chen, R. Clark, T. Dilbeck, Y. Zhou, J. Hurley, J. Neu, T. Besara, T. Siegrist, P. Djurovich and B. Ma, *ACS Appl. Mater. Interfaces*, 2017, **9**, 44579–44583.
48 D. Di Nuzzo, L. Cui, J. L. Greenfield, B. Zhao, R. H. Friend and S. C. J. Meskers, Circularly Polarized Photoluminescence

from Chiral Perovskite Thin Films at Room Temperature, *ACS Nano*, 2020, **14**, 7610–7616.

49 J. Ma, C. Fang, C. Chen, L. Jin, J. Wang, S. Wang, J. Tang and D. Li, Chiral 2D perovskites with a high degree of circularly polarized photoluminescence, *ACS Nano*, 2019, **13**, 3659–3665.

50 M. Wang, Z. Yang and C. Zhang, Polarized Photoluminescence from Lead Halide Perovskites, *Adv. Opt. Mater.*, 2021, **9**, 2002236.

51 D. Täuber, A. Dobrovolsky, R. Camacho and I. G. Scheblykin, Exploring the Electronic Band Structure of Organometal Halide Perovskite via Photoluminescence Anisotropy of Individual Nanocrystals, *Nano Lett.*, 2016, **16**, 5087–5094.

52 J. Liu, F. Hu, Y. Zhou, C. Zhang, X. Wang and M. Xiao, Polarized emission from single perovskite $FAPbBr_3$ nanocrystals, *J. Lum.*, 2020, **221**, 117032.

53 D. Täuber, A. Dobrovolsky, R. Camacho and I. G. Scheblykin, Bright triplet excitons in caesium lead halide perovskites, *Nature*, 2018, **553**, 189–193.

54 W.-G. Lu, X.-G. Wu, S. Huang, L. Wang, Q. Zhou, B. Zou, H. Zhong and Y. Wang, Strong Polarized Photoluminescence from Stretched Perovskite-Nanocrystal-Embedded Polymer Composite Films, *Adv. Opt. Mater.*, 2017, **5**, 1700594.

55 P. Satapathy, P. K. Santra and S. K. Prasad, Synergistic Path for Dual Anisotropic and Electrically Switchable Emission From a Nanocomposite of $CsPbBr_3$ Quantum Cuboids and Nematic Liquid Crystal, *Crystals*, 2019, **9**, 378.

56 D. Wu, D. Dong, W. Chen, J. Hao, J. Qin, B. Xu, K. Wang and X. Sun, Polarized emission from $CsPbX_3$ perovskite quantum dots, *Nanoscale*, 2016, **8**, 11565–11570.

57 X. Sheng, G. Chen, C. Wang, W. Wang, J. Hui, Q. Zhang, K. Yu, W. Wei, M. Yi, M. Zhang, Y. Deng, P. Wang, X. Xu, Z. Dai, J. Bao and X. Wang, Polarized Optoelectronics of $CsPbX_3$ (X = Cl, Br, I) Perovskite Nanoplates with Tunable Size and Thickness, *Adv. Funct. Mater.*, 2018, **28**, 1800283.

58 Y. Zhou, J. Luo, Y. Zhao, C. Ge, C. Wang, L. Gao, C. Zhang, M. Hu, G. Niu and J. Tang, Flexible Linearly Polarized Photodetectors Based on All-Inorganic Perovskite $CsPbI_3$ Nanowires, *Adv. Opt. Mater.*, 2018, **6**, 1800679.

59 L. Chen, M. Wang, B. Cao, S. Zhou, Y. Lin, J. Hu, C. Wang, J. Wang, Q. Sun and K. Xu, Highly linearly polarized white light emission from InGaN light-emitting diode with nanograting-integrated fluorescent ceramics, *Appl. Phys. Express*, 2017, **10**, 012101.